EXAMPLES OF X-RAY TOPOGRAPHIC RESULTS

A. MATHIOT
Departement de Metallurgie
Centre d'Etudes Nucleaires
85X - 38041 GRENOBLE CEDEX - FRANCE

INTRODUCTION

X ray diffraction by crystals has been extensively described former in this book and the aim of this contribution is, once the principles have been recalled, to look at the possible uses for the X ray topographic tool. We shall first outline the most important characteristics of the topographic image and then try to show some typical applications of these techniques. This review cannot be exhaustive, because the fields of application as well as the users are becoming increasingly numerous, since its invention by Lang in 1958(1). In particular the advent of synchrotron radiation facilities opened recently a new field for this tool, owing to the extremely intense white spectrum available. This paper will be confined to classical transmission topography, and the reflection techniques as well as the double crystal assessments will not be reviewed here. However the interested reader can have a look at the comprehensive reviews on that subject by Lang(2), Authier(3) or Tanner(4). Some specific applications will be described in order to show that X ray topography can be used either as a characterization technique for the study of defects in nearly perfect crystals or as a tool for a deeper investigation of elastic fields inside the crystal by means of models and simulation.

CHARACTERISTICS OF THE X RAY TOPOGRAPHIC IMAGE

The origin of the image lies in a perturbation of the ray trajectories inside the crystal due to the presence of elastic displacements. Those displacements arise from singularities in the crystal lattice configuration. So the contrast of the image is mainly due to defects and the size of the image is strongly dependent on the amplitude and derivatives of the elastic displacement.
As has been shown by Malgrange(5) the kinematical image is created from the direct beam in strongly distorted regions so that its size is usually quite small (a few microns). The dynamical image, due to perturbations inside the Borrmann fan of the wave field propagation in less distorted regions, is generally much larger than the kinematical one and can reach 100μm or more.
From the size of the images two important limitations arise for the study of defects: the resolution limit cannot be better than 1μm and practically will be of the order of 5 to 10μm. This is why it will not be possible by this technique to look conveniently at crystals containing more than a few defects (maximum dislocation density $10^4 cm^{-2}$). This means that applicability of X ray topography is restricted to quite perfect crystals.
To balance these disadvantages the interests of the tool are that it is non-destructive and that it can manage with quite macroscopic samples (a few cm^2 in surface and 50μm to few mm in thickness).

The exposure time is strongly dependent on the source used as well as on the detector (6). As an example the exposure time required for a Lang traverse topograph with a high brilliancy rotating anode X ray generator on a moderately absorbing crystal can be of the order of 10h/cm , if recorded on a nuclear plate. The same image can be obtained in 1mn with the white synchrotron radiation at LURE-DCI (1.8GeV, 100mA) and can also be recorded directly with poor resolution on a TV detector (exposure time 0.04sec).

X RAY TOPOGRAPHY AS A CHARACTERIZATION TOOL

The few following examples will try to show the variety of fields open to the topographic techniques in materials science.

1.CRYSTAL GROWTH

Looking at the local strains inside the crystal allows the experimentalist to follow the growth habit from the nucleation, to understand the growth mechanisms and to rebuild the growth history of the sample.

A-Naturally occurring crystals(7,8,9)

The non-destructive study of diamond by Lang(10) is one of the most beautiful applications in that field. X ray topography is able to show the strain field inside the crystal without slicing it off. Fig. 1 shows a section topograph through a slightly rounded natural diamond of about 5mm edge length, with axis [001] vertical. The natural growth faces in diamond correspond usually to octahedral growth sectors with {111} facets and cuboid rounded surfaces with mean orientation {100}. The sample presented here was enveloped in a layer of coat which prevented optical observation. The section passes 0.75mm distant from the center of the crystal. The areas appearing very dark on the print represent zones of non-faceted growth which are densely populated by minute bodies of unidentified composition. Due to local strain these bodies produce intense diffraction contrast from the matrix surrounding them.

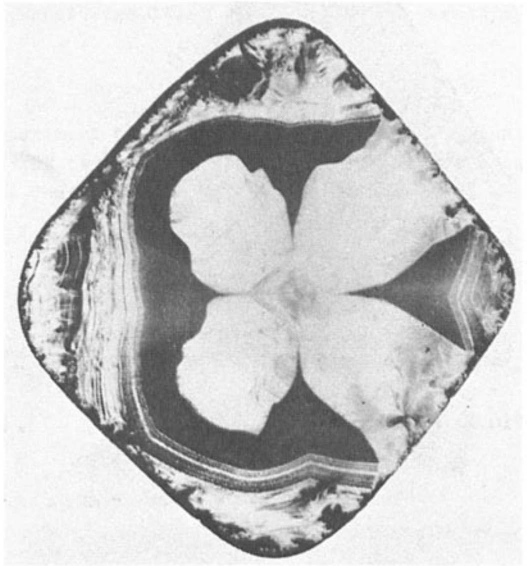

Fig.1: Section topograph through a natural diamond; reflection $\bar{4}04$, MoKα

B-Synthetic crystals grown from aqueous solution(11,12)

X ray topography is widely used in order to determine the optimal growth parameters in crystals. Fig. 2 to 4 show the results obtained by Gits-Leon & al.(13) on the effect of stirring on the quality of solution grown potash alum. The crystals are obtained by the temperature decrease of a saturated mother solution of potash alum (from 40 to 25°C). The seeds are (001) platelets cut from a previous crystal,

which are kept moving in the bath to obtain a constant flux velocity. Fig. 2 shows the main characteristics of the growth and the crystallographic orientation of the samples:

-The {111} and {001} facets appear simultaneously.

-The growth rate of the {001} facets is governed by the existence of screw dislocations. These dislocations are nucleated on local stress concentrations due to impurity segregation on the growth front (on the seed or on inclusions as at I).

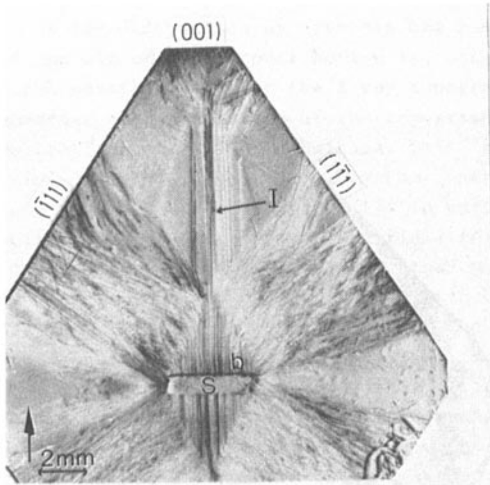

Fig.2: Potasn alum
$\bar{2}2\emptyset$ topograph, MoKα

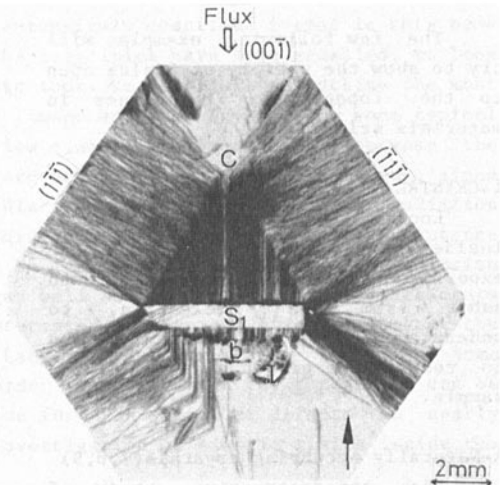

Fig.3: Potash alum; $\bar{2}2\emptyset$ topograph MoKα showing tne influence of flux direction

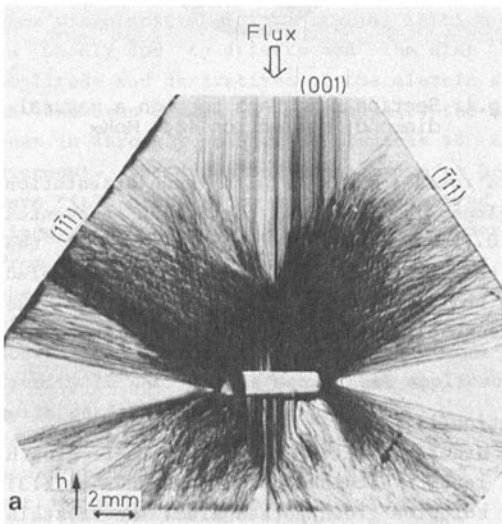

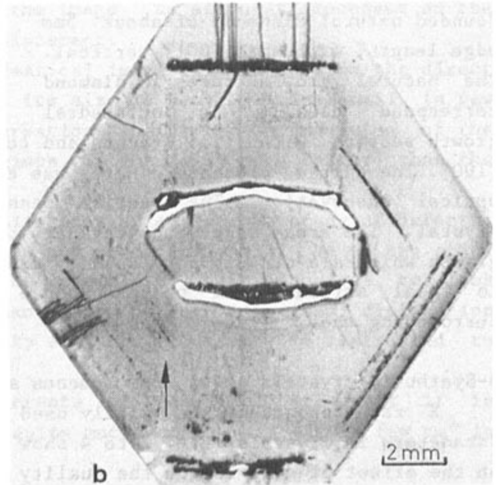

Fig.4: Influence of flux velocity on perfection. $2\bar{2}\emptyset$ topographs, MoKα. a) V=14 cm/sec b) V=0

-When these dislocations meet the limit between two growth sectors they are "refracted" in order to follow a normal to the growth front.

The variations in growth rate explain the fact that the {001} facets alternatively appear and disappear on the growth habit of the crystal. Fig. 3 shows the influence of the flux direction on the growth habit. The dislocations are mostly visible in front of the flux. In the back sectors, due to turbulence inside the liquid, the supersaturation may vary so that liquid inclusions can be embedded in the solid. They stop the dislocation propagation, and the crystal perfection looks better with the {001} facets growing slower and wider. Fig. 4 shows the influence of flux velocity on the quality of the crystals. On fig. 4a the relative velocity is 14cm/sec, when on fig. 4b it is zero. For high speeds the dislocation density is higher, many among them being of edge character do not contribute to the growth. For low speeds fewer dislocations and more inclusions are visible, due to a reduction of the solution exchange near the growing crystal, resulting in a better crystalline quality.

C-Dynamic study of recrystallization(14).

Fig. 5 shows an example of in-situ experiment by mean of synchrotron radiation. A slice of high purity aluminium, after a 3% critical strain, is heated directly in front of the beam, between 300 and 400 °C. The rearrangement of dislocations gives rise to small nuclei of perfect crystal. The recrystallization proceeds by the growth of those seeds at the expense of the deformed matrix. These grains are of random orientations and the fact that the incident beam is polychromatic allows to get Laue spots for some of them, corresponding to appropriate Bragg reflections. So that it is possible to follow the growth by recording these spots which are in fact topographic images on a film behind the furnace. Topographs of fig. 5 have been obtained by exposing X ray films 10sec every 3mn. They show the expansion of the grain by low indices facets and the interaction of these facets with neighbouring recrystallized grains, which results in a deformation of the growth habit (fig. 5c & d).

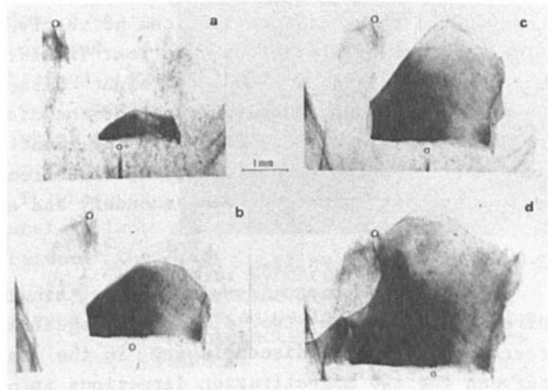

Fig.5: Synchrotron radiation topographs of Al recrystallization showing the first stages of a crystal growth

2. SYSTEMATIC STUDY OF DEFECTS IN CRYSTALS

A-Grain boundary dislocations(15).

Germanium bicrystals are a good model for a systematic study of grain boundaries. X ray topography is used here as a complement of electron microscopy, then it allows the examination of macroscopic samples on a larger scale. Apart from the so-called primary grain boundary dislocations of the classical Frank model for small angle grain boundaries, two types of dislocations are visible on fig. 6:

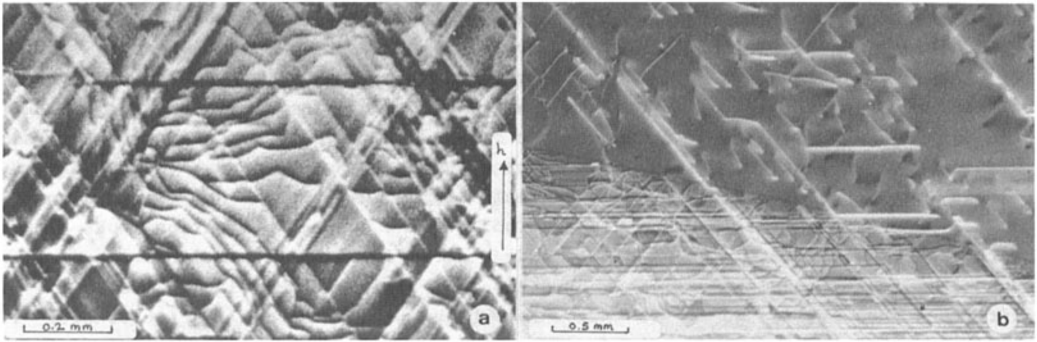

Fig.6: Grain boundary dislocations in Germanium. 400 reflection, MoKα
a) Secondary dislocations b) Extrinsic and matrix dislocations

-For special disorientations between the two crystals the total elastic energy is minimum; these particular respective orientations correspond to high densities of sites in coincidence position for both lattices. The crystals shown here can be superposed by a rotation of angle 38.94° around [110] which correspond to a twin index $\Sigma=9$. The so-called secondary dislocations account for a small deviation from the exact coincidence orientation in the same way as for primary dislocations in a small angle boundary. Their spacing D is related to their Burgers vectors b (which are quite smaller than those of primary dislocations) and to the deviation angle $\Delta\theta$ by the well known Frank relation: $D\times\Delta\theta=b$. When $\Delta\theta$ is very low as in fig. 6a ($\Delta\theta\leq0.005^\circ$) these dislocations can be resolved on X ray topographs.
-The extrinsic dislocations are matrix dislocations which end up on the grain boundary and then follow a straight direction which is the intersection of the boundary plane and the glide plane of the dislocation. This trapping by the boundary is clearly visible on fig. 6b. The identification of these dislocations is in progress(16) but some difficulties arise from the numerous reactions which take place on the boundary plane between secondary and extrinsic dislocations.

B-Magnetic domain walls.

In two adjacent domains of a single crystal two different magnetization directions produce two different magnetostrictive deformations. The domain wall corresponds to a discontinuity in the magnetoelastic field(17). When the angle between the two magnetization directions is not 180° this elastic singularity results in a contrast on X ray topographs(18), which allows a study of the domain configuration in magnetic samples.

Fig. 7 shows the evolution of domain structure in a (110) slice of ferrimagnetic Terbium-Iron garnet ($Tb_3Fe_5O_{12}$, TbIG) at low temperatures(19). In TbIG magnetization, magnetic anisotropy and magnetostriction increase notably when the temperature is lowered. This comes from a progressive reorientation of the magnetic moments in the ferrimagnetic lattice(20). As the domain number is roughly proportional to the square of the magnetization, it can be seen on fig. 7 that the wall images (vertical straight lines) become increasingly numerous for low temperatures. Moreover the

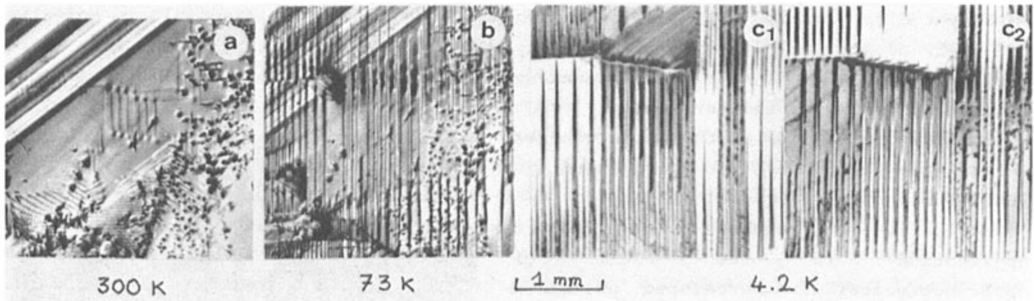

Fig.7: Evolution of domain structure in TbIG with temperature
$\overline{4}4\overline{4}$ reflection, MoKα

magnetostrictive deformation increases so that the departure from Bragg angle(5) may become larger than the width of the rocking curve. For such cases (fig. 7c) the Bragg peak splits into two parts, so that one can obtain two distinct complementary topographic images of the crystal, each of them corresponding to one set of domains with parallel magnetization. The measurement of this splitting allowed a direct determination of the magnetostriction coefficient for this garnet(21).

Another striking example of domain wall study is shown on fig. 8. This is a dynamic experiment performed at LURE-DCI(22). By means of an alternative magnetic field(80Hz) the domain walls in this Fe-3%Si crystal are vibrating and a stroboscopic topographic image is obtained by integration on a fixed phase. The wall images appear thin enough in the whole sample, which seems to prove the reversibility of the wall motion. An instability can be noticed at point P, where a precipitate is embedded in the crystal. This indicates an elastic interaction between the precipitate and the oscillating wall. The systematic study of such interactions between walls and defects is in progress.

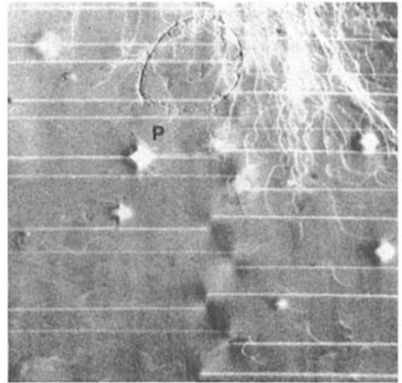

Fig.8: Synchrotron radiation stroboscopic image of oscillating walls in Fe-Si crystal Interaction with precipitate at P.

3. APPLICATION TO ELECTRONICS

As a non-destructive method X ray topography is widely used during the processing of electronic devices and correlated with electrical fault analysis.

Topograph of fig. 9 represents a (111) silicon wafer during the fabrication of integrated circuits(23). The surface has been oxidized and the oxide layer has been removed by etching on selected square areas. Then a phosphorus diffusion has been performed at high temperature(1050°C). Three characteristic sets of defects are visible and can be correlated with the electrical properties of the device:

-Emitter edge dislocations due to stress relaxation at the edge of the oxide layer, which run parallel to the surface from one edge to another one.

-Straight dislocations (lines along <110> and <112> directions) which limit stacking faults in the {111} planes, running likewise parallel to the surface.
-Extended defects inside the oxide windows which have been shown to correspond to local phosphorus overconcentrations.

Fig. 10 corresponds to another application in the field of optoelectronics(24). Deuterated potassium dihydrogenphosphate (D-KDP) is used as electro-optical modulator in optical relays which allow the transfer of an electronic, X ray or visible image by means of local variations of the refraction index due to an electric charge pattern. This device is mentioned by Clair in this book. The topographic image of the D-KDP crystal (fig. 10a) shows some dislocations and four growth sectors corresponding to growth along [001] and [010] directions (vertical and horizontal) through {110} facets. Those defects are electrically active and produce a damage in the stored image shown on fig. 10b after a few tens of seconds.

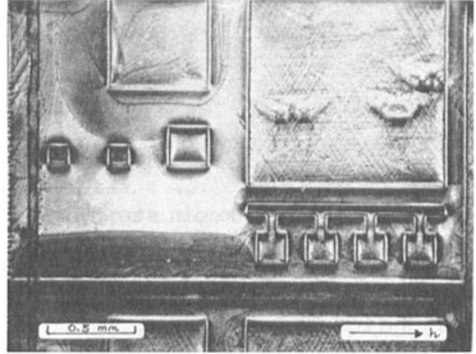

Fig.9: Silicon with oxide windows and P diffusion, 440 reflection, MoKα

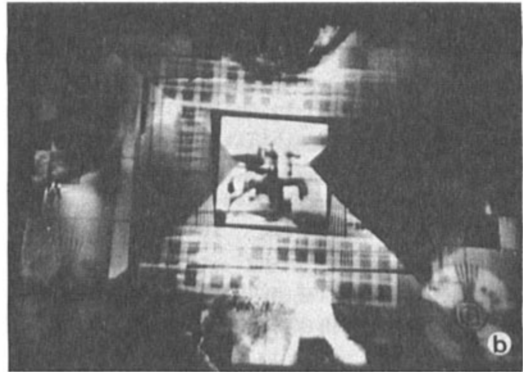

Fig.10: a) X ray topography of D-KDP single crystal with growth defects
b) Damage on the TV image electrically stored in the crystal due to the defects

X RAY TOPOGRAPHY AS A TOOL FOR INVESTIGATION

Three examples are given to show that this technique can help for the quantitative investigation of elastic fields in the crystal when it is possible to give a model for the distortion inside the crystal.

1. SILICON WITH SUPERPOSED OXIDE FILM (25)

As it has been mentioned above the oxide layer on silicon single crystals produces local stress concentrations which can be relaxed during heat treatment by

emission of dislocations. These stresses are due to a lattice difference between layer and substrate. A model of this deformation has been built and section topographs show a perturbation of the Pendellösung fringes with appearance of new elliptical fringes. This perturbation arises from the small strain gradient introduced in the substrate by the oxide film. These dynamical images can be analyzed in terms of the Eikonal theory, by computing the wave-field trajectories inside the Borrmann fan. Starting from the elastic model of the deformation this computation gives the exact phase integral for each wave-field and results in the fringes positions at the exit surface of the crystal. A comparison with the experimental positions, as measured on the section topographs for different oxide film thicknesses allowed a determination of the force per film unit length, and an evaluation of the stress inside the film.

2. CONTRAST OF A Y SHAPED MAGNETIC DOMAIN WALL JUNCTION (26)

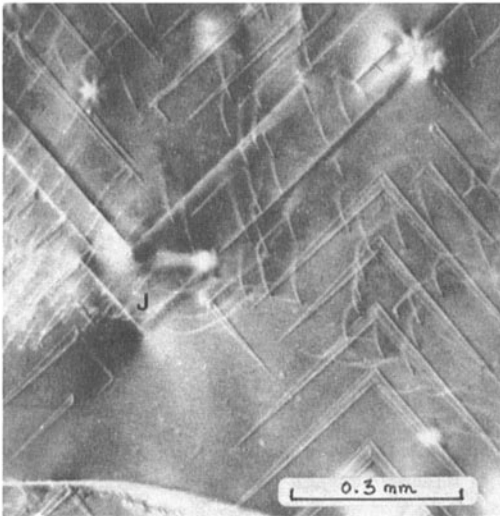

Fig.11: Domain walls in Fe-Si single crystal. Y shaped junction at J. 020 reflection, MoKα.

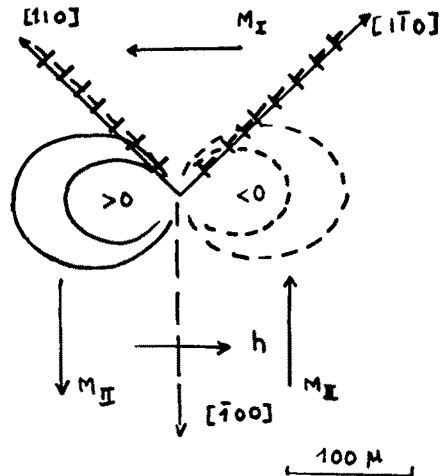

Fig.12: Representation of the junction, same orientation as fig.11; M_I & M_{II}: magnetization; solid and dashed curves are equi-G; h= diffraction vector

The magnetic domain wall configuration in Fe-3%Si at equilibrium exhibit a lot of junctions between two or three walls(fig. 11). The Y shaped junction consists in two 90° {110} walls and one 180° {100} wall (point J on fig. 11, fig. 12). The dynamical contrast of such junctions can be described with the help of continuous theory of dislocations(27) as the intersection of two planar quasi-dislocations densities (with infinitesimal Burgers vector) along the 90° walls. These walls produce an incompatible state of deformation (due to the differences in magnetostrictive deformation) which is equivalent to the presence at the junction of a wedge disclination of angle $3\lambda_{100}$, where λ_{100} is the magnetostriction coefficient. Starting from this model it is possible to compute the total displacement field and the strain gradient G which governs the dynamical contrast for such small deformations. Taking into account the surface relaxation the equi-G curves have been plotted (fig. 12) and correspond fairly well to the image's shape. Thus the disclination model of the junction is in good agreement with the experimental results.

3. CROSS SLIP OF ISOLATED DISLOCATIONS ON THE SURFACE OF SILICON CRYSTALS (28)

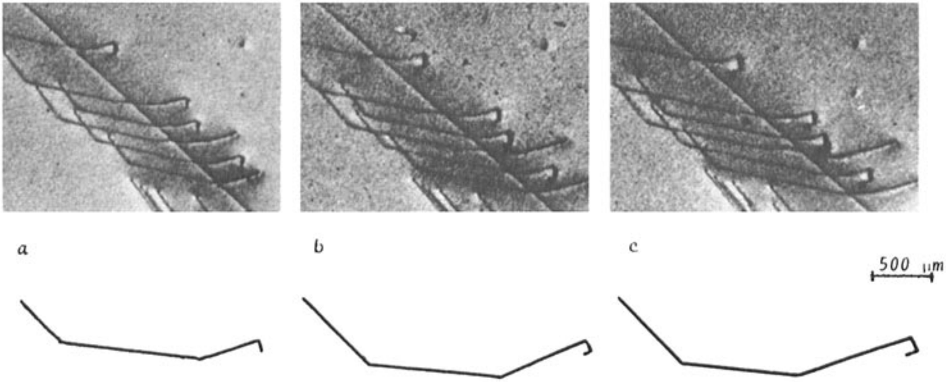

Fig.13: Cross slip of isolated dislocations on silicon surface. 2$\bar{2}$0 reflection, MoKα .

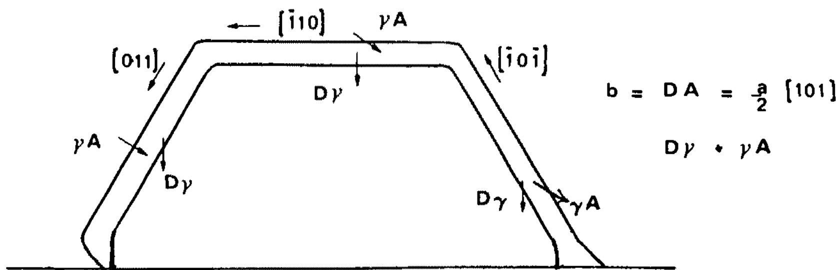

Fig.14: Geometry of the dislocation loop when dissociated

The study of plastic deformation and dislocation movement is one of the very interesting applications of X ray topography. On the surface of a dislocation free silicon crystal a scratch can act as a source of hexagonal half loops of dislocations during a high temperature tensile experiment. The movement of such dislocations can be followed by X ray topography. Moreover in-situ experiments are now in progress with the synchrotron radiation at LURE-DCI. Under specific conditions one can observe, as shown on fig. 13, that the half loops exhibit cross-slip near the surface. This phenomenon can only be interpreted in terms of dissociated dislocations. Fig. 14 shows the geometry of the loop in its (11$\bar{1}$) glide plane. The Burgers vector is 1/2[101], one segment is a pure screw, the two others are 60° dislocations. If the loop is dissociated in two Shockley partials with Burgers vectors 1/6[112] and 1/6[2$\bar{1}$1], surrounding an intrinsic stacking fault ribbon, the geometry is that of fig. 14. Electron microscopic observations have shown on Cu-Al that, near the surface, the partials tend to a screw orientation(29), which results in a narrowing or widening of the fault ribbon as shown on fig. 14. This configuration has been shown to be energetically favourable. This explains that the segment where both the dissociation width is narrower and the two partials have a dominant screw component can easily cross-slip. This last example shows that a lot of microscopic informations can be obtained on the basis of the macroscopic results from X ray topographs.

CONCLUSION

This brief review of X ray topography applications to materials science was not complete at all. But the aim was, above all, starting from various examples, to show the most important fields where it can help. As it is mostly sensitive to elastic fields, this technique has first been used as a characterization tool for the defects' study. But the current developement of simulation procedures allows deeper studies whenever elastic models can be built. Furthermore the recent appearance of intense, tunable polarized sources allows to foresee a lot of new applications both for the investigation of diffraction processes in crystals and for the study of dynamic phenomena.

REFERENCES

(1) LANG A.R.(1958) J. Appl. Phys. 29, 597
(2) LANG A.R. Diffraction and Imaging Techniques in Material Science. Amelincks, Gevers, van Landuyt eds. North-Holland(1978)
(3) AUTHIER A. X Ray Optics. Queisser ed. Topics in Applied Physics Vol.22, Springer(1977)
(4) TANNER B.K. X Ray Diffraction Topography, Int. Ser. Sc. Sol. St. Vol.10, Pergamon(1976)
(5) MALGRANGE C. This book
(6) COISSON, MILTAT : this book
(7) LANG A.R.(1974) J. Cryst. Growth 24/25, 108
(8) SAUVAGE M. and AUTHIER A.(1965) Bull. Soc. Fr. Min. Crist. 88, 379
(9) ZARKA A.(1974) J. Appl. Cryst. 7, 453
(10) SUZUKI S. and LANG A.R.(1976) Diamond Research 1976 p.39
(11) AUTHIER A.(1972) J. Cryst. Growth 13/14, 34
(12) IZRAEL A., PETROFF J.F., AUTHIER A. and MALEK Z.(1972) J. Cryst. Growth 16, 131
(13) GITS-LEON S., LEFAUCHEUX F. and ROBERT M.C.(1978) J. Cryst. Growth 44, 345
(14) GASTALDI J. and JOURDAN C.(1978) Phys. Stat. Sol.(a) 49, 529
(15) BACMANN J.J., MATHIOT A., SILVESTRE G. and DE TOURNEMINE R.(1977) IVth Eur. Cryst. Meet., Oxford p.646
(16) MATHIOT A. and GAY M.O. (to be published)
(17) CHIKAZUMI S. Physics of Magnetism, Wiley(1964)
(18) POLCAROVA M. and LANG A.R.(1962) Appl. Phys. Lett. 1. 13
(19) MATHIOT A. and PETROFF J.F.(1976) J. Appl. Phys. 47,1639
(20) NEEL L., PAUTHENET R. and DREYFUS B.(1964) Prog. Low Temp. Phys. 4, 344
(21) PETROFF J.F. and MATHIOT A.(1974) Mat. Res. Bull. 9, 319
(22) MILTAT J. private communication
(23) ROLLAND G. These 3eme cycle, Grenoble(1973)
(24) BELOUET C., DUNIA E. and PETROFF J.F.(1974) J. Cryst. Growth 23, 243
(25) KATO N. and PATEL J.R.(1973) J. Appl. Phys. 44, 965
PATEL J.R. and KATO N. ibid p.971
(26) MILTAT J.E. and KLEMAN M.(1973) Phil. Mag. 28, 1015
(27) KRONER E.(1958) Kontinuum Theorie der Versetzungen und Eigenspannungen. Springer
(28) GEORGE A. These d'Etat Nancy(1977)
(29) HAZZELDINE P.M. KARNTHALER H.P. and WINTNER E.(1975) Phil. Mag. 32,81